Coiled Coil in the Stalk Region of ncd Motor Protein Is Nonlocally Sustained

Mie Ito,[‡,§] Hisayuki Morii,*[,§] Takashi Shimizu,[§] and Masaru Tanokura[‡]

Graduate School of Agricultural and Life Sciences, The University of Tokyo, Yayoi 1-1-1, Bunkyo-ku, Tokyo 113-8657, Japan, and Institute for Biological Resources and Functions, National Institute of Advanced Industrial Science and Technology (AIST), Higashi 1-1-1, AIST-C6, Tsukuba, Ibaraqi 305-8566, Japan

Received July 27, 2005; Revised Manuscript Received December 1, 2005

ABSTRACT: The dimeric structure of kinesin superfamily proteins plays an important role in their motile functions and characteristics. In this study, the coiled-coil-forming property of the stalk region (192−346) of *Drosophila* ncd, a C-terminal kinesin motor protein, was investigated by synthesizing various peptide fragments. The α helicity of a set of 46-residue peptides spanning the stalk region appeared too low to form a coiled-coil dimer, probably because of insufficient continuity of the hydrophobic residues at (*a* and *d*) core positions in amphipathic heptad repeats. On the other hand, several peptides with leucine residues introduced at core positions or with extensional sequences with high α helicity had an advantage in coiled-coil formation. When we analyzed the thermal and urea-induced unfolding of these dimeric peptides, we identified four domains having a relatively high potential to form coiled coils. Among them, three domains on the C-terminal side of the stalk region, i.e., (252−272), (276−330), and (336−346), were in the same heptad frame, although these potential coiled-coil domains were not self-sustaining individually. This is in sharp contrast to the fragment of human kinesin, (332−369), which has an extremely high tendency toward coiled-coil formation. One of the possible triggers for coiled-coil formation of the ncd stalk region may be the interaction between the motor domain and the C-terminal part of the stalk as previously revealed by X-ray crystallography. The residues, S331 and R335, seem to act as a breaking point for α-helix continuity. This would make the region (336−346), as the head−stalk joint, more flexible such as seen with a plus-end-directed kinesin, if this region had no interaction with the motor domain. These characteristic differences between ncd and kinesin suggest that the nonlocally sustained coiled coil of ncd is one of the factors important for minus-end-directed motility.

The product of the nonclaret disjunctional gene of *Drosophila*, ncd, is a member of the kinesin superfamily, and its polypeptide chain is composed of 700 amino acid residues (*1*). It belongs to the kinesin-14 family, that is, the C-terminal motor subfamily with an α-helical coiled coil in the middle part and a tail at the N terminus. In contrast, most members of the kinesin superfamily have their motor domains at the N terminus. The three-dimensional structure of the ncd motor domain is very similar to that of *Homo sapiens* kinesin heavy chain (HsKHC)[1] (*2*, *3*). Kinesin superfamily proteins interact with microtubules and use the hydrolysis of MgATP to power the translocation of themselves and their cargos, such as organelles, along microtubules (*4*). Despite the structural similarity of the motor domains, ncd moves along a microtubule toward its minus end (*5*, *6*), whereas HsKHC moves toward its plus end (*7*). The dimeric structure of ncd is distinctly different from that of HsKHC, as revealed by not only X-ray crystallography but also low-angle X-ray and neutron scattering for the solution structure (*8*).

The stalk region extending from the motor domain to the cargo-binding domain has heptad repeats for both ncd and HsKHC. Such a region is thought to form an α-helical coiled coil to induce dimerization of the motor proteins. The positions of the heptad repeat characterizing the amphipathic helices are generally designated as *a*, *b*, *c*, *d*, *e*, *f*, and *g*, in which the first and the fourth positions, i.e., *a* and *d*, are allocated to the main periodic occurrence of hydrophobic residues (*9*). Several recent studies have suggested that the transition region between the motor domain and the coiled-coil stalk of kinesin family proteins is important in the motility directionality (*10*−*12*). We herein refer to this coiled-coil forming region as the "top-stalk", that is, the α-helical portion closest to the motor domain among individual α helices in a stalk region. In human kinesin, the top-stalk region (332−369) has been, in fact, shown to form a dimeric coiled-coil structure, which was estimated on the basis of the propensity scores for an amphipathic helix evaluated by our original method, "Amphisearch" (*13*).

Electron microscopic observations showed the truncated ncd constructs MC5 (the peptide consisting of the residues 295−700) and MC6 (333−700) to be dimeric and monomeric, respectively (*14*−*16*). X-ray crystallographic analysis also revealed that the region (303−346) of the motile ncd

* To whom correspondence should be addressed. Telephone: (+81)-29-861-6091. Fax: (+81)-29-861-9494. E-mail: morii.hi@aist.go.jp.

‡ The University of Tokyo.

§ National Institute of Advanced Industrial Science and Technology (AIST).

[1] Abbreviations: HsKHC, *Homo sapiens* kinesin heavy chain; Ac, acetyl; TBTU, 2-(1*H*-benzotriazol-1-yl)-1,1,3,3-tetramethyluronium tetrafluoroborate; HOBt, 1-hydroxybenzotriazole; NMM, *N*-methylmorpholine; CD, circular dichroism; ESI−MS, electrosprayed ionization mass spectroscopy; DTT, dithiothreitol; TFE, 2,2,2-trifluoroethanol.

10.1021/bi051480f CCC: $33.50
Published on Web 02/14/2006

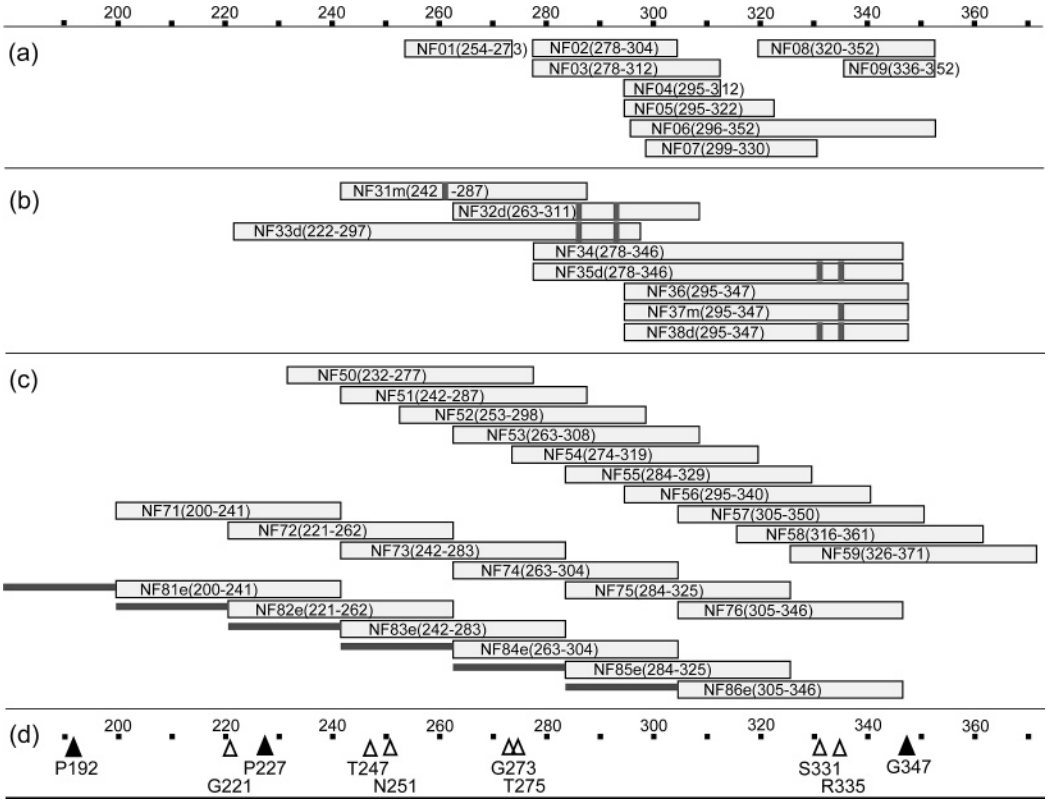

FIGURE 1: Schematic representation of the synthetic fragments on the scale of the residue number. The peptides were classified into three categories as shown in a−c, which are selected fragments with native sequences, the peptides for the mutation study, and systematic sequences, respectively. Every fragment has a code name, NFi, where i denotes the individual number. For the meaning of the characters attached, m, d, and e, see the Experimental Procedures. The bold marks indicate the mutation sites. The bars for NF80s represent the extensional sequence with amphipathic helicity, RE LKELEQK LKELEQK LKELY. The residues of the probable domain boundary as discussed in the text are shown with triangles (d). The solid triangles indicate the borders of a synchronous heptad frame shift.

dimer (281−700) forms a coiled coil (*17*). Interestingly enough, there have been reported two different X-ray crystallographic structures for dimeric ncd (*17*, *18*). One has 2-fold symmetry (PDB accession code 2NCD), and the other has a dissymmetric orientation of two motor domains (PDB accession code 1N6M). This polymorphic character implies that the stalk region plays an important role in the structural organization of the ncd motor protein.

In the present study, we first searched the entire stalk region to locate amino acid sequences that would potentially take coiled-coil structures by our statistical method based on a heptad amphipathy (*13*). On the basis of the propensity scores, we have synthesized various peptides of 17−76 amino acid residues and analyzed their structural properties by circular dichrosim (CD) spectroscopy. Our current work has focused not only on determining the coiled-coil potential of subregions of the stalk but also on clarifying the thermodynamic behavior of the stalk. Here, we describe that the potential coiled-coil regions were identified but that they were not self-sustaining. The consequence of this property is discussed in relation to ncd motility.

EXPERIMENTAL PROCEDURES

Prediction of Coiled-Coil Propensity. The amino acid sequence of ca. 400 residues for the N-terminal of the ncd polypeptide that was thought to contain a coiled-coil structure was evaluated by means of the algorithm named "Amphisearch" (*13*). The results for the profile of coiled-coil propensity were represented with seven curves.

Native and Modified Peptides. The synthesized peptides with the sequence of the stalk region are indicated in Figure 1. All peptides examined were named "NF", to which individual code numbers were appended as well as corresponding sequence numbers. Additional alphabetical codes, m, d, c, and e, represent "monosubstituted", "disubstituted", "coupled dimer", and "extensional-sequence conjugated", respectively. The region in the ncd sequence was denoted in each bar with residue numbers. All NF peptides were acetylated at the N terminus to reduce the effect of the electrostatic charge.

The mutation sites for NF31m(242−287), NF32d(263−311), NF37m(295−347), and NF38d(295−347) are at the hydrophobic core positions of a heptad repeat. Similarly, NF33d(222−297) and NF35d(278−346), covering wider regions of the sequence, have mutations of H286L/H293L and S331L/R335L, respectively. NF21e(295−326), NF22-(295−308/337−352), NF23(320−347/406−423), NF24-(335−347/406−423), NF26c(299−330), NF27c(299−330), and NF28c(335−347) are the peptides formed by the combination of two sequences (see the Supporting Information).

Each peptide from NF71(200−241) to NF76(305−346) bears an additional *N*-acetyltyrosine residue at the N terminus for convenience in the quantification. The peptides from NF81e(200−241) to NF86e(305−346) are conjugated at the N terminus with an extensional sequence acetyl (Ac)-RE LKELEQK LKELEQK LKELY named NF80e, which has a high potential to form a coiled-coil structure (see Figure

8b). This extension was attached to conserve the identical heptad frame with the succeeding native sequence.

Synthesis. Fmoc amino acids and the coupling reagents were purchased from Watanabe Chem. Ind. (Japan). The Sieber-amide resins (Novabiochem) were used to provide the peptides with amide-type C termini. The peptides were synthesized by the solid-phase method using a Shimadzu PSSM8 peptide synthesizer. Each peptide was elongated by a stepwise coupling reaction with 0.1 M Fmoc amino acid solution containing 2-(1*H*-benzotriazol-1-yl)-1,1,3,3-tetramethyluronium tetrafluoroborate (TBTU)−1-hydroxybenzotriazole (HOBt)−*N*-methylmorpholine (NMM) (1, 1, and 2 equiv of amino acid) reagent system for 30 min. The peptides were cleaved from the resin and purified in a manner similar to that described previously (*13*).

The concentration of the peptide solutions was determined with the ninhydrin reaction after acid hydrolysis (*19*). The molecular weights of synthetic peptides were measured by electrosprayed ionization mass spectroscopy (ESI−MS) with QP-8000 (Shimadzu). All of the peptides synthesized in this work were confirmed to be true products judged from small mass errors almost within unity. The molecular weights of representative peptides were as follows: NF33d(222−297), 8653.4 (theoretical, 8654.7); NF35d(278−346), 8126.4 (8126.3); NF37m(295−347), 6226.8 (6227.1); NF38d(295−347), 6253.2 (6253.2); NF56(295−340), 5524.9 (5525.2); NF71(200−241), 5247.8 (5246.9); NF76(305−346), 5298.3 (5298.0); and NF81e(200−241), 7754.1 (7753.9).

CD Measurement. The CD spectra in the far-UV region (186−260 nm) were recorded on a Jasco J-820 spectropolarimeter. Cylindrical quartz cuvettes with a 0.2−10 mm path length were used, and the temperature was controlled at 20 °C with a water-circulation system. The spectral data were collected in solutions of 50 mM K-phosphate buffer at pH 7.0 unless described otherwise. For cysteine-containing peptides, 1 mM dithiothreitol (DTT) was added to suppress oxidation. In some cases, 20% aqueous solution of 2,2,2-trifluoroethanol (TFE) was used as a helix-inducing solvent.

The temperature-scanning CD measurement was carried out by simultaneously monitoring the ellipticity and temperature. The heating rate was 1.0 K/min. The two-state transitions from a dimer to monomers were analyzed by curve fitting with thermodynamic equations given previously (*13*). However, some of the transition curves observed in the present work seemed to involve changes with more than two states; therefore, we analyzed them with the equations for a three-state transition derived from the comprehensive theoretical treatment by Kidokoro et al. (*20*, *21*), as indicated in the Appendix.

RESULTS AND DISCUSSION

Predictive Evaluation of the Propensity for Coiled-Coil Formation. Ncd contains a motor domain starting from Gly347 through its C terminus, K700 (*17*). The stalk region (192−346) extending from the motor domain has amphipathic heptad repeats (Figure 2) and is likely to be in a coiled-coil conformation. The remaining N-terminal part marked off at Pro192 is thought to form a cargo-binding domain. When we applied the method "Amphisearch" (*13*) to the stalk region of ncd, we obtained a profile of the propensity scores for coiled coils, as shown in Figure 3.

	a	b	c	d	e	f	g		a	b	c	d	e	f	g
192	P	Y	D	F	K	A	R	279	L	S	E	L	Q	A	I
199	F	H	D	L	L	E	K	286	H	E	K	V	K	T	E
206	H	K	V	L	K	T	K	293	H	A	A	L	S	T	E
213	Y	E	K	Q	T	E	D	300	V	V	H	L	R	Q	R
220	M	G	E	L	E	S	M	307	T	E	E	L	L	R	C
227					P	Q	Q	314	N	E	Q	Q	A	A	E
230	L	E	E	T	Q	N	K	321	L	E	T	C	K	E	Q
237	L	I	E	T	E	S	S	328	L	F	Q	S	N	M	E
244	L	K	N	T	Q	S	D	335	R	K	E	L	H	N	T
251	N	E	C	L	Q	R	Q	342	V	M	D	L	R	G	N
258	V	K	Q	H	T	A	K	349	I	R	V	F	C	R	I
265	I	E	T	I	T	S	T	356	R	P	P	L	E	S	E
272	L	G	R	T	K	E	E	363	E	N	R	M	C	C	T
								370	W	T					

FIGURE 2: Primary structure of ncd. The amino acid sequence of the probable stalk region with a part of the motor domain of ncd is shown. The amino acid residues are aligned on the basis of the heptad assignment from *a* to *g*. Among the residues at the *a* and *d* positions in the stalk region, the hydrophobic ones are shaded. The special glycine and proline residues are indicated with boxes.

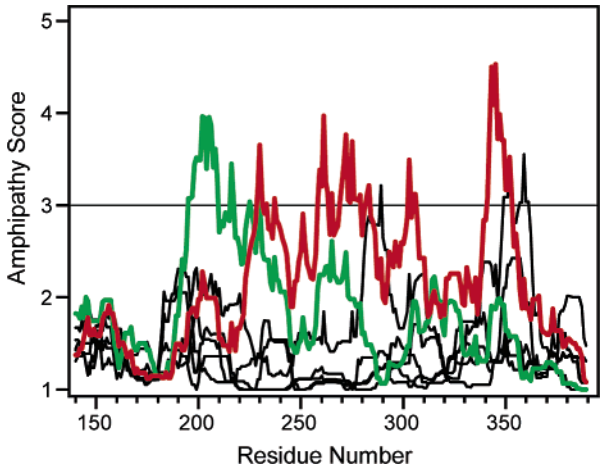

FIGURE 3: Profile of the propensity scores for the amphipathic helical structure. The scores were calculated for ncd with our originally developed program "Amphisearch" (*13*). Two patterns corresponding to heptad-(7N-1) and heptad-(7N-4) are indicated with red and green lines, respectively. The patterns for the other five types of heptads are shown in black.

The graphic representation of Amphisearch consists of seven curves corresponding to all seven types of heptad frame shift. Generally, the coiled-coil structure exhibits a characteristic distribution of these seven curves: a single curve has a high level and is accompanied by two curves with moderate scores (*13*). On the basis of our empirical data, we found the necessary condition for stable coiled-coil formation to be a score above 3 at a peak. When we judged from the quantitative assessment of the propensity scores of ncd using this criterion, we predicted that two regions would be prone to form coiled-coil structures. One is found in the region (225−355) as shown in red, (7N-1), in Figure 3. The other is the region (194−220) showing a high-score curve in green, which belongs to a different type of heptad frame shift, (7N-4). Therefore, the mismatch of these two types of heptad frame shifts may lead to a kink in the region containing Pro227.

The propensity score for ncd was at most 4.5 at position 344, while the top-stalk region (332−369) of human kinesin had a maximum score of 5.4 (*13*). The scores at other peak positions 202, 230, 261, and 272 were around 4.0 (Figure 3). These modest scores at the peaks, although larger than

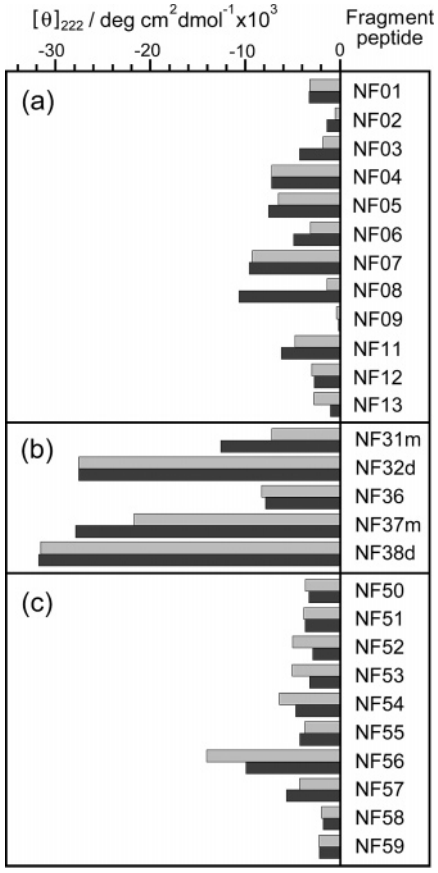

FIGURE 4: CD intensities at 222 nm for various ncd fragments. The molar ellipticities at 222 nm in 50 mM potassium phosphate buffer solution (pH 7.0) and those in the same buffer containing 500 mM KCl are shown with light and dark gray bars, respectively. The concentrations of the peptides were in the range of 0.2−0.4 mM. The code names of the fragments are indicated in the right column. The fragments are classified into a−c in the same manner as in Figure 1. The data for the peptides NF11(295−322), NF12-(299−315), and NF13(337−352) are added in category a.

3, may be ascribed to incomplete continuity of the hydrophobic residues at the core positions (*a* and *d*) of heptad repeats. The maximum number of such continuity of residues was only 3, as found in (Ile265, Ile268, and Leu272), (Leu296, Val300, and Leu303), and (Leu338, Val342, and Leu345) (Figure 2). Therefore, three representative regions around the positions 270, 300, and 340 were selected for the first phase of synthesis of the peptides (Figure 1a). In addition, systematic fragments with 46 and/or 42 residues were synthesized to survey coiled-coil formation along the whole sequence of the stalk (Figure 1c). These systematic peptides involve 13 and/or 12 residues occupying the (*a* and *d*) positions of heptad repeats. Because leucine zipper peptides are known to form stable coiled coils with, for example, 8 hydrophobic residues at 9 (*a* and *d*) positions (*22*), a similar number of hydrophobic residues at the core positions would be sufficient for coiled-coil formation. In fact, the top-stalk region of kinesin contains 9 hydrophobic residues at the total of 13 core positions.

CD Spectra of the Peptides with the Native Sequences of ncd. The CD spectra of the peptides covering the region (227−346) were measured, and the molar ellipticities at 222 nm are summarized in Figure 4. The intensities of molar ellipticity $[\theta]_{222}$ for most of the peptides with native sequences were weak and within −10 000° cm^2 dmol^{-1}, indicating that they had low or little α helicity. Only a few peptides from the region close to the motor domain, i.e., NF36(295−347), NF56(295−340), and NF07(299−330), showed slightly more intensive $[\theta]_{222}$ values as −8300, −14 100, and −9300° cm^2 dmol^{-1}, respectively.

The conformations of these native peptides were minimally dependent upon the concentrations from 0.001 to 0.6 mM (data not shown). Therefore, even if any of these peptides forms coiled coils, the dissociation constant (K_d) would be 1 mM or more, which is much different from K_d for the kinesin top-stalk fragment (332−369), 62 nM (*13*). This strongly suggests that no peptides from the native sequence with 46 residues or less in length form a coiled-coil structure at the physiological ionic strength.

To examine coiled-coil formation at a high effective concentration, we synthesized dimerized peptides NF26c-(299−330), NF27c(299−330), and NF28c(335−347); however, they showed no apparent increase in helical contents in comparison with the corresponding monomeric peptides. Additionally, the coiled-coil formations induced by the interaction between two separated regions were not observed for the linked peptides NF22(295−308/337−352), NF23-(320−347/406−423), and NF24(335−347/406−423).

Comparison of CD Spectra for 46-Residue Peptides Scanning the Stalk Region. We conducted a systematic search for a possible coiled-coil formation with a series of 46-residue peptides. NF50(232−277)−NF57(305−350), covering the region (232−350), as well as NF58(316−361) and NF59-(326−371), containing a part of the motor domain, were selected with their N-terminal residues corresponding to *c* or *f* positions of heptad repeats (Figure 1c). Each peptide contains 13 core (*a* and *d*) residues of heptad repeats. The number of hydrophobic residues at the (*a* and *d*) positions are 7, 8, 9, 9, 7, 8, 8, and 7 for NF50(232−277)−NF57-(305−350), respectively, which is nearly comparable to that of a leucine zipper sequence, such as GCN4 (*22*). The CD spectra showed that the patterns resembled each other, except for that of NF56(295−340) (Figure 5a). The molar ellipticities at 200 nm were about −20000° cm^2 dmol^{-1}, indicating random-coil structures. NF58(316−361) and NF59(326−371), containing the motor domain sequence, exhibited weaker molar ellipticities than NF50(232−277)−NF55(284−329).

Of this series of 46-residue peptides, only NF56(295−340) gave a CD pattern suggesting an α helix. Nevertheless, the intensity at 222 nm was −14 300° cm^2 dmol^{-1}, about half of the signal for a fully coiled-coil peptide such as NF38d(295−347). The α-helical region of NF56(295−340) was estimated to be ca. 20 residues in length. Interestingly, the temperature-scanning CD measurement revealed that NF56(295−340) underwent a very steep thermal transition, suggesting the structure formation of a highly cooperative nature. The thermal transition temperatures observed at the concentrations of 0.03 and 0.45 mM were 51.8 and 52.8 °C, respectively. The best-fitting parameters led to a prediction that the transition temperatures for the system of monomer−dimer equilibrium should be different by 6 K. This suggests that the α-helical structure of NF56(295−340) is not formed through monomer−dimer equilibrium. Such concentration-independent formation of an α helix was reported by one of the current authors for corticotropin-releasing factor, which had a special association mechanism among its monomer,

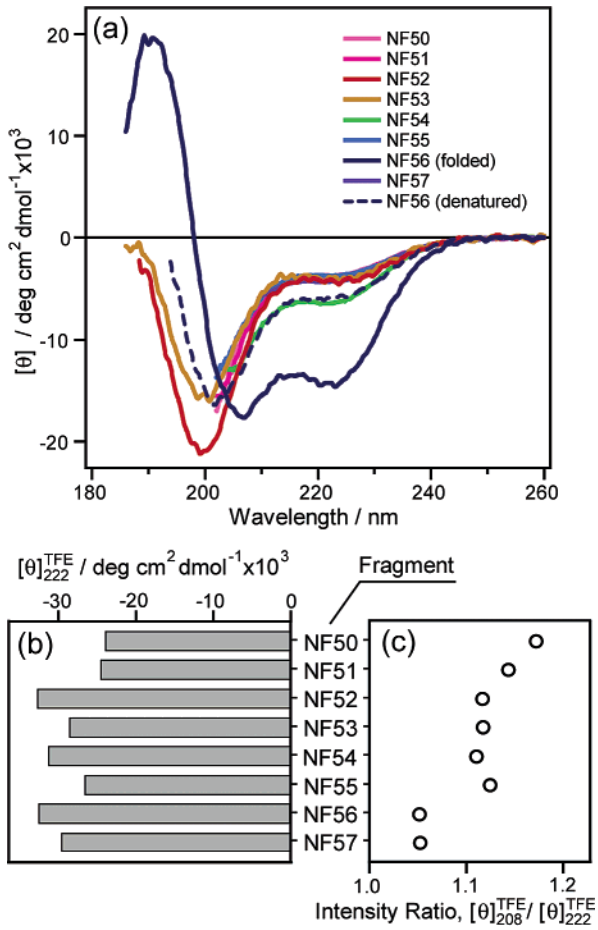

FIGURE 5: CD spectra of ncd fragments. (a) Spectra of a series of 46-residue peptides [NF50(232−277)−NF57(305−350)] are exhibited. The spectra were obtained at the peptide concentrations of 0.4−0.5 mM at 20 °C, except for NF56(295−340), which was measured at 10 °C. The spectrum of NF56(295−340) measured at 10 °C after thermal denaturation is shown with a broken line. (b) Molar ellipticities at 222 nm observed in 20% aqueous TFE solutions are shown. (c) Ratios of the molar ellipticities at 208 and 222 nm obtained from the spectra in 20% TFE solutions are plotted on the same axis as is used in b.

tetramer, and the micelle-like species (*23*). In the case of NF56(295−340), no association was found by the measurement for concentration dependence, so that the α-helix structure of NF56(295−340) was thought to be intramolecular. It should be noted that the CD spectrum of NF56(295−340) after thermal unfolding was quite similar to those of NF50(232−277)−NF55(284−329), indicating that it did not refold.

Effects of Solvent Conditions. As described above, the fragments of the ncd stalk region showed a low propensity for coiled-coil formation, in contrast to the top-stalk of human kinesin. In response to that, we investigated the effects of solvent conditions on structure formation. Although high ionic strength is generally expected to enhance hydrophobic interactions to promote coiled-coil formation, even the addition of 500 mM KCl resulted in similar molar ellipticities at 222 nm, as shown in Figure 4. Also, the presence of Zn^{2+} is known to cause a large increase in the stability of α-helical Zn^{2+}-binding proteins (*24*, *25*). However, NF50(232−277)−NF55(284−329) and NF31m(242−287), which include His261, His286, and His293 at the (*a* and *d*) positions, resulted in no apparent increase in α-helical contents in the presence of Zn^{2+} or Mg^{2+} ions (data not shown).

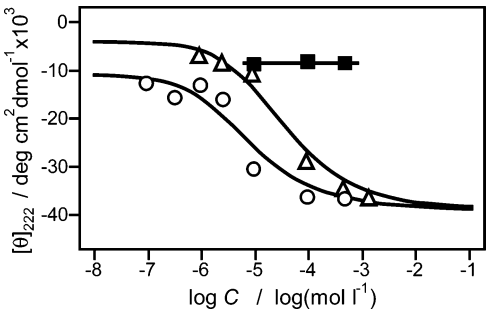

FIGURE 6: Concentration dependence of molar ellipticities at 222 nm. The molar ellipticities of NF36(295−347), NF37m(295−347), and NF38d(295−347) are plotted with ■, △, and ○, respectively. The best-fitted theoretical curves calculated on the basis of monomer−dimer equilibrium are superimposed on the plots. The dissociation constants for NF37m(295−347) and NF38d(295−347) were found to be 32 and 7.3 μM, respectively. The end level at a high concentration was taken to be −39 000° cm^2 dmol^{-1} as an extrapolated value.

Alcoholic aqueous solutions are known to be favorable for the α-helix structure (*26*). In fact, the CD spectra of NF50(232−277)−NF57(305−350), a series of 46-residue peptides, in 20% TFE exhibited a typical pattern of an α helix with the molar ellipticity at 222 nm around −30 000° cm^2 dmol^{-1}, suggesting the potential propensity for α-helix formation of the stalk region (Figure 5b). A characteristic difference was found in the ratio of molar ellipticities at 208 and 222 nm, $[\theta]_{208}/[\theta]_{222}$, which would reflect a higher-order feature of an α helix (Figure 5c). These ratios for NF56(295−340) and NF57(305−350) were distinctively small, 1.05, in contrast to the values of 1.12−1.15 for NF51(242−287)−NF55(284−329). The small value of this ratio, often found for a coiled-coil peptide such as NF35d(278−346) shown below in Figure 7a, suggests that the sequence for NF56(295−340)−NF57(305−350) would be prone to form a coiled coil. Probably, this would be ascribed to its relatively large number of hydrophobic residues at the positions other than (*a* and *d*) of heptad repeats.

Effects of Mutation on Dimerization. In the stalk region, there exist three pairs of hydrophilic residues at neighboring (*a* and *d*) positions, (Thr247 and Asn251), (Asn314 and Gln317), and (Ser331 and Arg335). To evaluate the instability caused by these polar residues and the extent of inductive coiled-coil formation, we examined the leucine mutants for some of those hydrophilic residues.

NF37m(295−347) is the R335L mutant of NF36(295−347), and NF38d(295−347) has an additional mutation, S331L/R335L. The concentration dependence of molar ellipticities for these peptides is shown in Figure 6. In contrast with NF36(295−347), both NF37m(295−347) and NF38d(295−347) exhibited remarkable concentration-dependent changes in CD intensities at 222 nm, reflecting monomer−dimer equilibria. The quantitative evaluation by the method of Chen et al. (*27*) suggests that nearly entire sequences have highly α-helical coiled-coil structure. On the basis of the curve-fitting analysis, we estimated the dissociation constants for NF37m(295−347) and NF38d(295−347) to be 32 and 7.3 μM, respectively. Thus, a single leucine substitution at Arg335 was highly effective in inducing and stabilizing these coiled coils. In other words, the charged Arg335 residue interferes significantly with the coiled-coil formation.

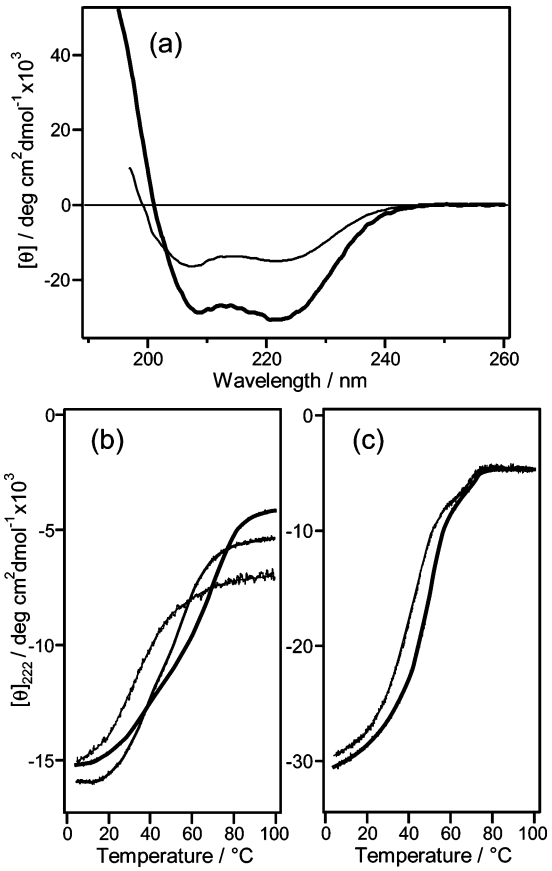

FIGURE 7: CD spectra and thermal transition curves of the mutant peptides. (a) Spectra of NF33d(222−297) and NF35d(278−346) are shown with thin and bold lines, respectively. The concentrations were 0.35 and 0.10 mM, respectively. (b) Thermal transition curves of NF33d(222−297) are shown. The data were analyzed with a three-state model (see the Appendix). The theoretical curves for different peptide concentrations, i.e., 0.35, 0.029, and 0.002 mM, are indicated with bold, regular, and thin curves, respectively. (c) Thermal transition curves of NF35d(278−346) are shown. The theoretical curves of a two-state model at the peptide concentrations of 0.10 and 0.010 mM are represented with bold and thin curves, respectively.

Long peptides, NF33d(222−297) and NF35d(278−346), were designed similarly with leucine substitutions. They were H286L/H293L for NF33d(222−297) and S331L/R335L for NF35d(278−346), which were located at the positions close to their C termini. The CD spectra indicated that these peptides were highly α-helical (Figure 7a). Especially, NF35d(278−346) appeared to form a nearly complete coiled-coil structure. Because the corresponding native peptide NF34(278−346) exhibited less than half of the CD intensity at 222 nm for NF35d(278−346), the induced coiled-coil structure extends from the substitution sites at Ser331 and Arg335 by almost 50 residues. This suggests that the coiled-coil structure in a wide region, (278−330), can be brought about by a local trigger sequence even for a long sequence.

Similar leucine substitutions at the (*a* and *d*) positions, H261L and H286L/H293L, were carried out to make NF31m(242−287) and NF32d(263−311), respectively. The CD spectra of these mutants exhibited remarkable enhancement in α helicity in comparison with those of the corresponding native sequences (parts b and c of Figure 4 and Figure 5a). These results can be ascribed to the increase in the continuity of hydrophobic residues at (*a* and *d*), from 3 to 6 residues for NF31m(242−287) and from 3 to 8 residues for NF32d(263−311).

The peptide NF32d(263−311) showed fully α-helical structure, in contrast with NF33d(222−297), forming a partial α helix despite having the same leucine substitutions. The trigger-induced coiled-coil formation as found in highly α-helical NF35d(278−346) did not take place for NF33d-(222−297). The hydrophilic residues, Thr247 and Asn251, at the adjacent core positions would disrupt the possible trigger-induced coiled-coil formation. Thus, by means of leucine substitutions, it was revealed that Arg335 and Thr247/Asn251 are significantly unfavorable for the connectivity of the coiled-coil formation.

Thermal Transition of Mutant Fragments. The thermal transitions of NF33d(222−297) and NF35d(278−346) were investigated at various peptide concentrations. NF33d(222−297) exhibited two transitions in the temperature range employed (Figures 7b). Upon reduction of the peptide concentration from 0.35 to 0.029 mM, the apparent temperature of the transition for NF33d(222−297) occurring at the higher temperature shifted from ca. 70 to 55 °C. This concentration-dependent transition should be attributed to dimer−monomer dissociation. On the other hand, the apparent transition at the lower temperature was independent of the peptide concentration; therefore, it could be assigned to a structural change in the dimer but not to dissociation. This is clearly proven by the curve-fitting calculation on the basis of monomer−dimer equilibrium involving a partial transition at a lower temperature (Figure 7b). The transition temperatures obtained, T_{d1} and T_{d2}, for NF33d(222−297) were (38.2 and 106.6 °C), (36.1 and 102.7 °C), and (30.1 and 107.5 °C) at the concentrations of 0.35, 0.029, and 0.002 mM, respectively. In the calculation, T_{d2} was defined as the transition temperature of dissociation extrapolated to 1 M concentration as a standard. Thus, each of the two transition temperatures was in a relatively narrow range irrespective of the concentrations, showing the validity of this three-state transition model. When we compared the extent of molar ellipticity changes at 222 nm for these two transitions, we were able to determine that the one at the higher temperature (ca. 105 °C) occupied 60% of the total change. This percentage corresponds to about 23 residues in the C-terminal half of NF33d(222−297), which is a probable α-helix region, as mentioned above. When the amino acid sequence is taken into account, Gly273 or Thr275 at the *d* position would be a possible break point in the helical region of NF33d(222−297).

On the other hand, the thermal transition of NF35d(278−346) occurred as a single event around 40 °C (Figure 7c). This transition temperature was dependent upon the peptide concentration. Therefore, the thermal transition of NF35d-(278−346) reflected the monomer−dimer equilibrium, the transition temperature of which was calculated to be 89 °C at the concentration of 1 M. When these results were combined, we concluded that a long region of the stalk with about 70 residues from positions 276 to 346 undergoes a cooperative transition, when the coiled-coil structure is induced at its C-terminal part.

Induction of a Coiled Coil by Extensional Sequence. Because coiled coils can be formed by the induction from short sequences at terminal regions as described above, evaluation of intrinsic coiled-coil propensity may be possible

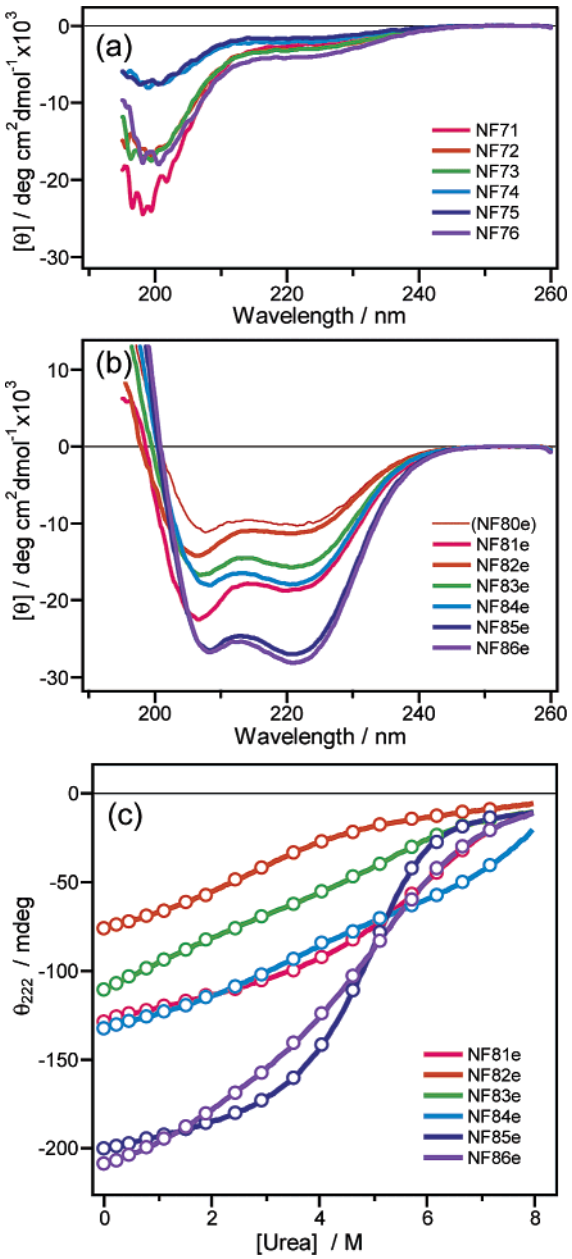

FIGURE 8: CD spectra of systematically selected fragments and their urea-induced transition curves. The color coding is indicated in the inset legend. (a) CD spectra of a series of 43-residue fragments. The concentrations of the peptides were 0.2 mM. (b) CD spectra of a series of fragments bearing an extensional sequence with helix-forming ability are exhibited. The CD spectrum of NF80e, which is a 21-residue peptide with the sequence of the extensional region only, is superimposed, of which the molar ellipticity is shown as a imaginary 63-residue peptide for the sake of comparison with the other 63-residue peptides, NF80s. Therefore, the actual CD spectrum of NF80e has a 3-fold intensity of that shown in this figure. (c) Urea-induced transition curves of the peptides NF81e(200−241)−NF86e(305−346) are shown. The CD intensities at 222 nm are plotted with ○, and the theoretical curves are superimposed. The theoretical equations for the transition curves are described in the Supporting Information.

by using conjugated peptides of the native sequence and a 20-residue sequence of a de novo designed coiled coil. The CD spectra of the peptides NF71(200−241)−NF76(305−346) indicate random-coil structures (Figure 8a), which are similar to the other peptides shown in parts a and c of Figure 4. On the other hand, the same peptides conjugated with the designed α-helical extensional sequence NF81e(200−241)−NF86e(305−346) showed CD spectra with α-helical characteristics (Figure 8b), although the extent varied depending upon the sequences.

Among these conjugated peptides, the molar ellipticity $[\theta]_{222}$ of NF82e(221−262) was the least intensive, −11 000° cm^2 dmol^{-1}, which is comparable to the value of NF80e with the sequence corresponding to the extensional region. Pro227 in the native sequence is likely to inhibit the continuity of the α helix. The molar ellipticities at 222 nm of NF83e(242−283) and NF84e(263−304) were −15 600 and −17 700° cm^2 dmol^{-1}, respectively, suggesting that the induced α-helical regions were partial in the native sequences. The lengths of α-helical regions were estimated to be 9 and 13 residues in addition to the extensional sequence for NF83e(242−283) and NF84e(263−304), respectively. Therefore, the probable amino acid residues to interfere with α-helix formation are thought to be the polar residues at the *a* and *d* positions, that is, Asn251 for NF83e(242−283) and Thr275 for NF84e(263−304).

In contrast, the peptides NF85e(284−325) and NF86e(305−346) exhibited remarkably intensive molar ellipticities at 222 nm, indicating that these peptides were nearly, at least, complete α helices. As the native sequences of NF85e(284−325) and NF86e(305−346) are included in that of NF35d(278−346), the high tendency for α-helix formation of these two is consistent with the result for NF35d(278−346). It should also be noted that the continuous polar residues at the *a* and *d* positions, Asn314 and Gln317, are not breaking points for the α helix. These may form intermolecular hydrogen bonds such as the asparagine residues in GCN4 (*22*).

To reveal the domain structures in NF81e(200−241)−NF86e(305−346), we carried out urea titration experiments (Figure 8c). The peptide NF82e(221−262) forming a coiled coil only at the extensional sequences underwent denaturation at a urea concentration of 8.9 M with the transition free energy (ΔG_{H_2O}) of 33.5 kJ/mol, where the values are those at the reduced peptide concentration of 1 M. In contrast, highly α-helical NF85e(284−325) showed a sharp transition at a urea concentration of 8.9 M with a ΔG_{H_2O} value of 53.5 kJ/mol. This transition could be assigned to a cooperative one of the native and extensional sequences. The peptides NF83e(242−283) and NF84e(263−304) did not appear to undergo simple two-state transitions. The transition curve of NF86e(305−346) was somewhat dull, although its molar ellipticity was comparable to that of NF85e(284−325). This implies that NF86e(305−346) consists of at least two domains.

Cross-Match Test for the Peptides with Extensional Sequences. In the stalk region of the intact ncd protein, there may exist some interactions to form coiled coils between different subregions. To assess heterodimer formations resulting from such interactions, we carried out a CD measurement of a mixed solution of two equimolar peptides from NF81e(200−241)−NF86e(305−346). The molar ellipticities are summarized in Figure 9 as the relative values from the geometrical averages of the corresponding two individual peptide solutions. It was notable that $[\theta]_{222}$ values of the heterogenic systems containing NF81e(200−241) or NF85e(284−325) were generally enhanced from those averaged for corresponding homodimers. The α helicity induced by NF81e(200−241) or NF85e(284−325) may be ascribed

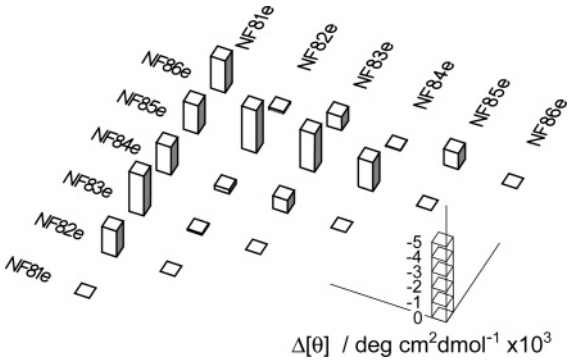

FIGURE 9: Changes in CD intensities by cross-mixing of the fragment peptides. The cross-match test was carried out for every pair from NF71(200−241)−NF76(305−346) and/or NF81(200−241)−NF86(305−346). After equimolar solutions of two kinds of peptides were mixed and dried in vacuo, the resulting solid was dissolved in a buffer solution and then the CD spectrum was measured at a concentration of 0.2 mM. The changes of molar ellipticities at 222 nm, $\Delta[\theta]$, are shown as a three-dimensional block graph. The values of $\Delta[\theta]$ were calculated by subtracting the averaged molar ellipticity of the components from the observed one for the mixed system. For example, the block indicated at the position (NF81e and NF85e) shows the difference, $[\theta]_{(NF81e + NF85e)} - ([\theta]_{(NF81e)} + [\theta]_{(NF85e)})/2$. The values at the orthogonal positions are null to show a control.

to the formation of the related heterodimers. Interestingly, these two peptides resulted in a sharp transition in urea-induced unfolding, as described above. Thus, the hetero- and homodimeric coiled-coil formations from the subregions are possible in the stalk. Although homodimeric coiled coils would be relatively stable in a static condition, heterodimeric coiled coils may have some contribution to the dynamic process from unwound states, which involves the interaction between local sites.

CONCLUSIONS

When the results are summarized, we can draw the following conclusions regarding the coiled-coil formation of the ncd stalk region (192−346): (i) There are no partial peptides with up to 46 residues with the ability to self-sustain coiled coils in the stalk region. (ii) Nonetheless, there exist several regions with a potential to form coiled coils by induction from neighboring regions. They are the regions (193−226), (252−272), (276−330), and (336−346), which are separated by probable breaking residues, Pro192, Pro227, Thr247/Asn251, Gly273/Thr275, Ser331/Arg335, and Gly347. These are polar amino acid residues at the *a* and *d* positions or proline and glycine residues. Among them, the discontinuation for cooperative coiled-coil formation is not very strict at Thr247/Asn251 and Gly273/Thr275. (iii) Because the three regions (252−272), (276−330), and (336−346) have the same synchronized periodicity of an amphipathic heptad, the formation of a continuous coiled coil with up to 95 residues would be possible. (iv) There exists a domain in the region (295−340) that could form an intramolecular helical structure. (v) Coiled-coil formation between heterogenic sequences is possible. Such a tendency is relatively high for the peptides, NF81e(200−241) and NF85e(284−325), related to the regions (193−226) and (276−330).

The ability to form a local self-sustaining coiled coil is low in the ncd stalk region in comparison with that of human kinesin. However, the coiled-coil formation of the sequence

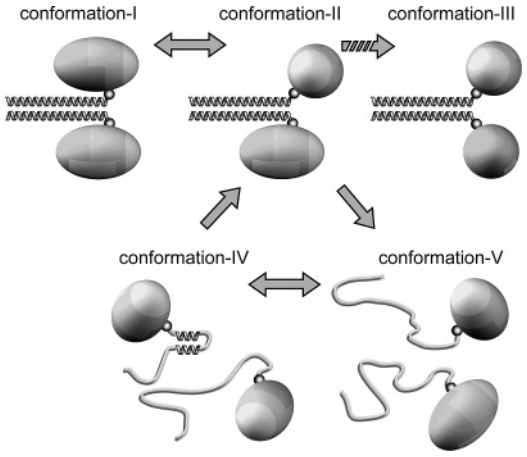

FIGURE 10: Illustration of probable conformations. Each drawing shows a different conformation of a couple of ncd motors. The motor domain and the stalk region are depicted with a spheroid and a helical ribbon or a deformed string, respectively. The small sphere represents Gly347. Conformations I and II are schematic representations of X-ray crystallographic structures, which were taken from 2NCD and 1N6M in the Protein Data Bank, respectively (*17*, *18*). Conformation III is imaginary, which is discussed in the text. Conformation IV is drawn on the basis of the result for NF56-(295−340), showing intramolecular coiled-coil formation. The random-coil stalk region brings about a monomeric form of ncd with conformation V.

from around 300 to 346 is reported in X-ray crystallographic studies (*17*). It should be noted that the region (325−346) of the stalk interacts with the surface of the motor domain at multiple points. When the crystallographic results as well as our findings are taken into account, we believe that this interaction may be an important trigger for coiled-coil formation.

Recently, two distinctive 3D forms of ncd motor domains dimerized by the top-stalk coiled coil, (303−346) or (293−346), were revealed (*17*, *18*). One is symmetric, with the top-stalk region interacting with both of the motor domains. Another has a dissymmetric form, in which either motor domain is twisted against the top-stalk coiled coil (*18*). These structures can be schematically illustrated as conformations I and II in Figure 10, respectively. The finding of conformation II means that the top stalk does not always interact with both of the motor domains. This may lead to a hypothetical structure, conformation III, bearing no interactions between the coiled coil and either motor domain. However, our results on the fragments suggest that conformation III is unstable, especially in the case of a stalk less than 50 residues in length. If the ncd molecule could take conformation III, the degree of freedom for the relative positions of both motor domains would be fairly high. This conformation resembles the dimeric form of human kinesin in terms of flexibility, because the latter has at least two residues (334−335) as a potentially flexible joint between the top stalk and the motor domains (*28*). Endow et al. (*29*) working with chimeric mutants have reported that the motility directionality along the microtubule does not depend upon whether the motor domain is derived from human kinesin or from ncd. Therefore, a motor protein in conformation III would be plus-end-directed. Because the hypothetical conformation III of ncd is considered to be unstable, as discussed above, it is reasonable to consider that ncd does not move toward the plus end of a microtubule.

As a joint of the stalk and the motor domain, ncd has Gly347, which is thought to act like a pivot. The dihedral angles (ϕ, ψ) of Gly347 in conformation I are (166°, −87°), as calculated on the basis of X-ray crystallographic data. The nontwisted motor domain in conformation II shows dihedral angles of (123°, 129°). Generally, these (ϕ, ψ) angles are allowed in the energy map only for glycine residue. On the other hand, the dihedral angles of the twisted motor domain in conformation II are (−123°, −172°), which are in the possible range even for usual α amino acids. Thus, the glycine residue at position 347 is indispensable for the conformations with the interaction between the stalk and the motor domain, which are conformation I and the nontwisted half of conformation II.

These findings show that both the relatively weak propensity for self-sustaining coiled coil and Gly347 are essential for the characteristic conformations of ncd, in which a motor domain would be constrained into a few orientations by the partner motor domain. Our preliminary analysis for other C-terminal motor proteins implies that their capabilities for forming a self-sustaining coiled coil are also relatively low. Additionally, the long synchronized amphipathic heptad with about 100 residues from the joint Gly347 should be noted as the top stalk with regard to its conformational characteristics and to the directionality in the movement along a microtubule.

APPENDIX

Thermodynamic Equations for Three-State Transition. We assumed the three states of our systems to be a folded dimer, a partially unfolded dimer, and unfolded monomers, which were coded as 0, 1, and 2, respectively, in the following expressions. According to the usual treatment, the measure for the transition such as molar ellipticity is expressed with the linear combination of the contribution from these three states as eq 1. The six parameters, a_0, a_1, a_2, b_0, b_1, and b_2, were introduced at first as shown in eq 2 on the assumption that three intrinsic values for these states, i.e., y_0, y_1, and y_2, can be approximated with linear functions of a variable such as temperature (T).

$$y = y_0 f_0 + y_1 f_1 + y_2 f_2 \tag{1}$$

$$\begin{aligned} y_0 &= a_0(T - T_{01}) + b_0 \\ y_1 &= a_1(T - T_{01}) + b_1 \\ y_2 &= a_2(T - T_{01}) + b_2 \end{aligned} \tag{2}$$

The molar fractions, f_0, f_1, and f_2, of these states are expressed with the functions z_{01} and z_{12}, consisting of transition free energies, as shown in eqs 3−5.

$$\begin{aligned} f_0 &= \frac{1 - z_{12}}{1 + z_{01} - z_{12}} \\ f_1 &= \frac{z_{01}(1 - z_{12})}{1 + z_{01} - z_{12}} \\ f_2 &= \frac{z_{01} z_{12}}{1 + z_{01} - z_{12}} \end{aligned} \tag{3}$$

$$z_{01} = \exp\left(\frac{-\Delta G_{01}}{RT}\right) \tag{4}$$

$$z_{12} = \frac{1}{8}\left\{\sqrt{\exp\left(\frac{-\Delta G_{12}}{RT}\right)\left[16 + \exp\left(\frac{-\Delta G_{12}}{RT}\right)\right]} - \exp\left(\frac{-\Delta G_{12}}{RT}\right)\right\} \tag{5}$$

The free-energy changes, ΔG_{01} and ΔG_{12}, are expressed with the thermodynamic parameters, that is, transition temperature (T_{01} and T_{12}), partial heat capacity change (ΔC_{p01} and ΔC_{p12}), and transition enthalpy (ΔH_{01} and ΔH_{12}), as well as the peptide concentration (C), as shown in eqs 6 and 7 (*20*, *21*).

$$\Delta G_{01} = \left[(1 + \ln T_{01})\Delta C_{p01} - \frac{\Delta H_{01}}{T_{01}}\right]T - \Delta C_{p01} T \ln T + (\Delta H_{01} - T_{01}\Delta C_{p01}) \tag{6}$$

$$\Delta G_{12} = \left[(1 + \ln T_{12})\Delta C_{p12} - \frac{\Delta H_{12}}{T_{12}}\right]T - \Delta C_{p12} T \ln T + (\Delta H_{12} - T_{12}\Delta C_{p12}) + RT \ln\left(\frac{C}{2}\right) \tag{7}$$

The observed curves for thermal transitions were analyzed by the least-squares method with these equations.

The urea-induced unfolding was analyzed essentially in the same manner as above except for the use of several different parameters and equations as described below. The intrinsic three states are expressed with linear functions of the concentration of urea, x_{urea}, as eq 8 instead of eq 2. Also, the functions z_{01} and z_{12} were differently defined as eqs 9 and 10, respectively.

$$\begin{aligned} y_0 &= a_0 x_{urea} + b_0 \\ y_1 &= a_1 x_{urea} + b_1 \\ y_2 &= a_2 x_{urea} + b_2 \end{aligned} \tag{8}$$

$$z_{01} = \exp\left(\frac{-\Delta G_{u01}}{RT}\right) \tag{9}$$

$$z_{12} = \frac{1}{4C}\left\{\sqrt{\exp\left(\frac{-\Delta G_{u12}}{RT}\right)\left[8C + \exp\left(\frac{-\Delta G_{u12}}{RT}\right)\right]} - \exp\left(\frac{-\Delta G_{u12}}{RT}\right)\right\} \tag{10}$$

The transition free energy, ΔG_u, was expressed with two parameters, ΔG_d and m, according to the usual linear-dependent model as follows:

$$\begin{aligned} \Delta G_{u01} &= \Delta G_{d1} - m_1 x_{urea} \\ \Delta G_{u12} &= \Delta G_{d2} - m_2 x_{urea} \end{aligned} \tag{11}$$

SUPPORTING INFORMATION AVAILABLE

Formation of peptides by the combination of two sequences. This material is available free of charge via the Internet at http://pubs.acs.org.

REFERENCES

1. Endow, S. A., Henikoff, S., and Soler-Niedziela, L. (1990) Mediation of meiotic and early mitotic chromosome segregation in *Drosophila* by a protein related to kinesin, *Nature 345*, 81−83.

2. Sablin, E. P., Kull, F. J., Cooke, R., Vale, R. D., and Fletterick, R. J. (1996) Crystal structure of the motor domain of the kinesin-related motor ncd, *Nature 380*, 555−559.
3. Kull, F. J., Sablin, E. P., Lau, R., Fletterick, R. J., and Vale, R. D. (1996) Crystal structure of the kinesin motor domain reveals a structural similarity to myosin, *Nature 380*, 550−555.
4. Vale, R. D. (2003) The molecular motor toolbox for intracellular transport, *Cell 112*, 467−480.
5. Walker, R. A., Salmon E. D., and Endow S. A. (1990) The *Drosophila* claret segregation protein is a minus-end directed motor molecule, *Nature 347*, 780−782.
6. McDonald, H. B., Stewart, R. J., and Goldstein, L. S. B. (1990) The kinesin-like ncd protein of *Drosophila* is a minus end-directed microtubule motor, *Cell 63*, 1159−1165.
7. Vale, R. D., Reese, T. S., and Sheetz, M. P. (1985) Identification of a novel force-generating protein, kinesin, involved in microtubule-based motility, *Cell 42*, 39−50.
8. Kozielski, F., Svergun, D., Zaccai, G., Wade, R. H., and Koch, M. H. J. (2001) The overall conformation of conventional kinesins studied by small-angle X-ray and neutron scattering, *J. Biol. Chem. 276*, 1267−1275.
9. Parry, D. A. (1982) Coiled-coils in α-helix-containing proteins, *Biosci. Rep. 2*, 1017−1024.
10. Henningsen, U., and Schliwa, M. (1997) Reversal in the direction of movement of a molecular motor, *Nature 389*, 93−96.
11. Case, R. B., Pierce, D. W., Hom-Booher, N., Hart, C. L., and Vale, R. D. (1997) The directional preference of kinesin motors is specified by an element outside of the motor catalytic domain, *Cell 90*, 959−966.
12. Wendt, T. G., Volkmann, N., Skiniotis, G., Goldie, K. N., Müller, J., Mandelkow, E., and Hoenger, A. (2002) Microscopic evidence for a minus-end-directed power stroke in the kinesin motor ncd, *EMBO J. 21*, 5969−5978.
13. Morii, H., Takenawa, T., Arisaka, F., and Shimizu, T. (1997) Identification of kinesin neck region as a stable α-helical coiled coil and its thermodynamic characterization, *Biochemistry 36*, 1933−1942.
14. Chandra, R., Salmon, E. D., Erickson, H. P., Lockhart, A., and Endow, S. A. (1993) Structural and functional domains of the *Drosophila* ncd microtubule motor protein, *J. Biol. Chem. 268*, 9005−9013.
15. Hirose, K., Lockhart, A., Cross, R. A., and Amos, L. A. (1995) Nucleotide-dependent angular change in kinesin motor domain bound to tubulin, *Nature 376*, 277−279.
16. Hirose, K., Lockhart, A., Cross, R. A., and Amos, L. (1996) Three-dimensional cryoelectron microscopy of dimeric kinesin and ncd motor domains on microtubules, *Proc. Natl. Acad. Sci. U.S.A. 93*, 9539−9544.
17. Sablin, E. P., Case, R. B., Dai, S. C., Hart, C. L., Ruby, A., Vale, R. D., and Fletterick, R. J. (1998) Direction determination in the minus-end-directed kinesin motor ncd, *Nature 395*, 813−816.
18. Yun, M., Bronner, C. E., Park, C.-G., Cha, S.-S., Park, H.-W., and Endow, S. A. (2003) Rotation of the stalk/neck and one head in a new crystal structure of the kinesin motor protein, ncd, *EMBO J. 22*, 5382−5389.
19. McGrath, R. (1972) Protein measurement by ninhydrin determination of amino acids released by alkaline hydrolysis, *Anal. Biochem. 49*, 95−102.
20. Kidokoro, S., and Wada, A. (1987) Determination of thermodynamic functions from scanning calorimetry data, *Biopolymers 26*, 213−229.
21. Kidokoro, S., Uedaira, H., and Wada, A. (1988) Determination of thermodynamic functions from scanning calorimetry data. II. For the system that includes self-dissociation/association process, *Biopolymers 27*, 271−297.
22. O'Shea, E. K., Klemm, J. D., Kim, P. S., and Alber, T. (1991) X-ray structure of the GCN4 leucine zipper, a two-stranded, parallel coiled coil, *Science 254*, 539−544.
23. Morii, H., Uedaira, H., Ishimura, M., Kidokoro, S., Kokubu, T., and Ohashi, S. (1997) Special folding pathway to tetramer only through the micelle state of the corticotropin-releasing factor, *Biochemistry 36*, 15538−15545.
24. DeGrado, W. F., Summa, C. M., Pavone, V., Nastri, F., and Lombardi, A. (1999) De nove design and structural characterization of proteins and metalloproteins, *Annu. Rev. Biochem. 68*, 779−819.
25. Handel, T. M., Williams, S. A., and DeGrado, W. F. (1993) Metal ion-dependent modulation of the dynamics of a designed protein, *Science 621*, 879−885.
26. Hirota, N., Mizuno, K., and Goto, Y. (1997) Cooperative α-helix formation of β-lactoglobulin and melittin induced by hexafluoroisopropanol, *Protein Sci. 6*, 416−421.
27. Chen, Y.-H., Yang, J. T., and Chau, K. H. (1974) Determination of the helix and β form of proteins in aqueous solution by circular dichroism, *Biochemistry 13*, 3350−3359.
28. Kozielski, F., Sack, S., Marx, A., Thormählen, M., Schönbrunn, E., Biou, V., Thompson, A., Mandelkow, E. M., and Mandelkow, E. (1997) The crystal structure of dimeric kinesin and implications for microtubule-dependent motility, *Cell 91*, 985−994.
29. Endow, S. A., and Waligora, K. W. (1998) Determinants of kinesin motor polarity, *Science 281*, 1200−1202.

BI051480F